Transient Overvoltage Transfer and Amplification in a 400kV Network – A Case Study

S. K. E. Awadallah, S. Mohanty, F. Ghassemi

***Abstract*--The paper investigates overvoltage propagation in a 400kV network within the National Grid Electricity Transmission system in the UK. The studies were triggered by a replacement project for two parallel 400 kV cables and the installation of an additional one. The network in the vicinity of the cables has historical issues of flashover and circuit breaker failures. Electromagnetic transient studies were performed to simulate energisation and fault inception and clearance for the three new cables to examine compliance against overvoltage standards and limits. Studies were performed using the DIgSILENT analysis tool. Studies show that due to resonance in a specific frequency range, switching overvoltage propagated and amplified at remote nodes to a level close to the equipment's rated switching voltage. As mitigation, surge arresters with characteristics different from the National Grid recommended surge arresters were proposed and found suitable to bring the overvoltage values within the design limits for temporary overvoltage.**

***Keywords*: overvoltage, propagation, cables, electromagnetic transient, network resonance.**

I. Introduction

NATIONAL Grid Electricity Transmission (NGET) is undertaking several projects to replace some of its ageing assets and to reinforce the network to accommodate changes in the energy landscape. This paper reports a study that is triggered by one of these projects. The project involves the replacement of two parallel oil-filled 400 kV cables due to low asset health scores and the building of a third parallel 400 kV cable as identified by wider network studies for network reinforcement due to increased renewable generation. The area of the network where the project is undertaken has historical switching transient incidents. One of these incidents involved a trip of a super grid transformer (SGT) following the energisation of one of the cables under study, although the SGT is connected at a remote substation. Therefore, Electromagnetic Transient (EMT) studies were required to identify any issues and ensure the network and equipment in the vicinity of the project could endure any overvoltage resulting from switching events of these cables.

Transient overvoltage literature is full of practical studies discussing switching transient and Temporary Overvoltage (TOV) due to energisation or fault incidents on cables. Only a couple of them, however, reported overvoltage transfer and amplification to different nodes in the network other than the directly connected nodes. Reference [1], for example, investigated transient overvoltage due to fault initiation and clearance in an 1100 kV system where some of the investigated fault cases resulted in overvoltage levels of 1.4 pu on healthy parts of the studied network. Another example was reported in [2], where switching overvoltage studies were conducted to develop live working execution conditions for the Uruguayan transmission network. In one of the reported cases, an energisation of a 500kV line with a two-phase isolated fault led to a 2.3 pu overvoltage at a remote bus two substations away from the fault location. The study suggested connecting a metal oxide surge arrester at the impacted substation, which decreased the overvoltage level to 1.9 pu. Nonetheless, in both studies, propagation and amplification of overvoltage were not the main aims; hence no detailed investigation into the reasons behind the observations was included. This paper investigates the causes and analyses the network resonance and conditions where transient overvoltage is transferred and amplified. In addition to the time domain analysis, frequency scans were also carried out as part of the investigation to indicate the range of frequencies that might contribute to overvoltage. The studies and results presented in the paper serve as an example of overvoltage propagation and amplification on a realistic transmission network. The scope and steps of the studies would benefit future investigations into similar cases. It also enriches the literature with more examples of overvoltage transfer and amplification due to cable energisation (to levels that are higher than 2 pu).

EMT studies were carried out using the DIgSILENT power system analysis tool to investigate switching transient (slow front overvoltage) and Temporary Overvoltage (TOV) propagation in the 400 kV network. The effect of energising the three cables, fault inception, and clearance, was investigated, and the results were compared against National Grid's design recommendation. The network models and data are fully provided.

II. Compliance standards

A. Technical Specification (TS 1)

NGET's Technical Specification 1 (TS 1) is a document that gives National Grid's ratings and general technical requirements for plant, equipment, and apparatus for use in its electricity transmission system [3]. It defines the insulation level requirement for plants. For 400 kV voltage, the insulation level requirements for standard switching impulse withstand (SIL) voltage are 1050 kV peak for phase-to-ground (V_{ph}) peak voltage and 1575 kV for line-to-line (V_L) peak voltage.

S. K. E. Awadallah is with Texas A&M University at Qatar, Doha, Qatar (e-mail: selma.awadallah@ieee.org)
F. Ghassemi and S Mohanty are with National Grid plc, Warwick Technology Park, Gallows Hill, Warwick, CV34 6DA, UK (e-mails: forooz.ghassemi@nationalgrid.com and Somjit.mohanty@nationalgrid.com)

Paper submitted to the International Conference on Power Systems Transients (IPST2023) in Thessaloniki, Greece, June 12-15, 2023

B. Technical Guidance Note TGN(E) 288

Technical Guidance Note TGN(E) 288 defines the limits for Temporary Overvoltage (TOV) in England and Wales transmission network [4]. TGN 288 gives the limits for the changes in instantaneous voltage for planned and unplanned events which is 2.0 pu of the peak value of the system maximum continuous voltage, which is 420kV in this case. Thus, the instantaneous limits for the investigated network are 686 kV for V_{ph} voltage and 1188 kV for V_L voltage.

III. Modelling and EMT Simulations

Due to excessive modelling requirements and long simulation time for EMT studies, it is not practical to perform studies on the whole transmission network. Consequently, an area of the network around the cable installations was defined to perform the EMT studies. DIgSILENT built-in function for network reduction was used to reduce the network outside of the selected area to three equivalent boundary points.

A. Network Description

Fig.1 shows the network for EMT studies which includes 8 substations, 6 of which are 400 kV. Node A, Node F, and Node T2 are grid supply substations. Each of them has two step-down power transformers feeding a 132kV substation which is connected to an equivalent of the downstream distribution network. The network has three boundary points with the reduced network at Node B, Node C and Node T.

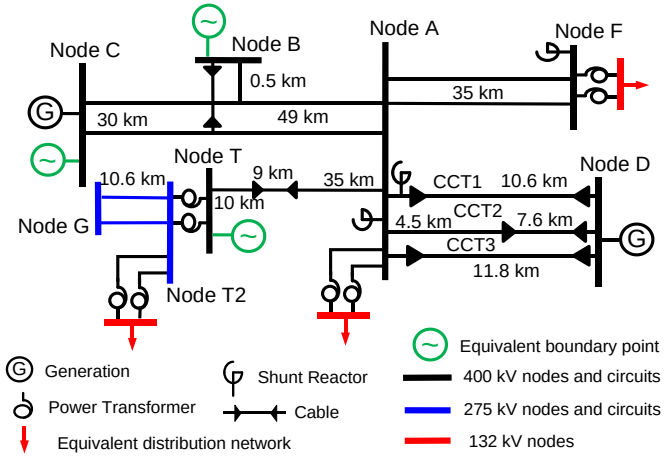

Fig.1. Selected network area for EMT studies

The project scope is to replace the two existing cables (CCT1 and CCT2) between Node A and Node D and add a third cable circuit (CCT3). While CCT1 is a 10.6km cable, CCT2 is a combination of a 7.3km cable and a 4.5km overhead line. The third circuit (CCT3) is an 11.6km cable circuit. CCT1 and CCT2 are shunt compensated by two 200Mvar reactors; one is directly connected with CCT1, and the other is connected to Node A's busbar. The third circuit increases the voltage across the area and leads to a requirement for a new reactive plant in the area, which will be connected to Node F, as shown in Fig.1. All equipment data is given in the Appendix.

B. EMT Modelling

1) Equivalent at Boundary Points

As per the recommendation in [5], the boundary points were considered at least one substation away from the point of interest. In addition, frequency scan analysis was completed using the whole network before reduction to detect resonance between the nodes where the cables are connected and nodes beyond the selected boundary points. The transfer coefficients from Node A and Node D to nodes beyond the boundary points were obtained by dividing the transfer impedance between nodes by the self-impedance of Node A or Node D. The results showed no evidence of high transfer coefficients. Fig. 2 shows an example of transfer coefficients between Node A and a node outside the boundary, i.e., in the reduced network. As seen, the transfer coefficient values do not indicate any significant propagation as the values are less than unity across the entire frequency range (100Hz to 3500Hz) except for the value at 2700 Hz, which is just above unity. This method was used to determine an effectively reduced network.

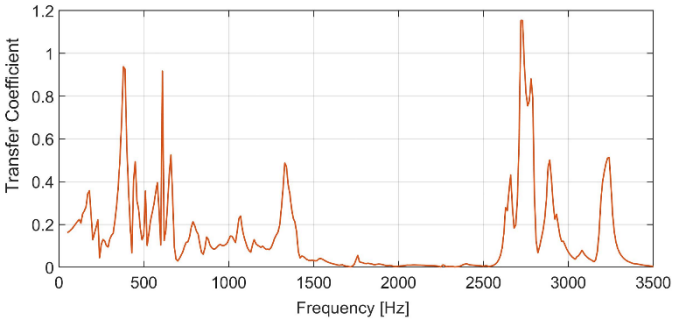

Fig. 2. Transfer coefficient from Node A to a node outside the boundary of network understudy at different frequencies

The reduced part of the network is modelled as Thevenin equivalent voltage source behind impedance at individual boundary points with positive and zero sequence impedances representing the reduced network.

2) Cables

The three cables under study were modelled using their geometry details provided in the cable data sheet, cable routes layout, and cross-bonding. The cables are directly buried in the ground in a trefoil formation; hence, no transposition is applied to the cables' conductors. Several sections of the cables are buried in the same trench (see Appendix). The cables are modelled using the Frequency Dependent Cable Model introduced in [6].

3) Overhead Lines

The overhead lines were modelled based on their geometry. Parallel circuits between the network nodes are all double circuits on the same towers. The overhead line part of CCT2 is coupled with part of the circuit between Node A and Node T. The Universal Line Model was used to model overhead lines.

4) Transformers

The core saturation curve characteristic was modelled using the polynomial representation available within DIgSILENT which has four parameters: knee flux, linear (unsaturated) reactance, saturated reactance, and saturation exponent. All transformers are 3 winding transformers with a tertiary winding voltage of 13kV and 60MVA capacity except transformers at Node T2 which are 2 windings transformers (275/132 kV).

5) Shunt reactors (200Mvar)

The core saturation was not considered because according to the reactor data sheet the core magnetic knee point is around 120% of the nominal voltage, which was deemed reasonably

high for switching overvoltage studies (the focus of this paper). High magnetic knee point has minimal impact on the slow front overvoltages, e.g., switching transients. The winding capacitance and iron loss were modelled as extra shunt elements connected to the reactor. The iron loss was assumed to be 0.05% of the rated reactive power as per [7,8]. The winding capacitance value was assumed to be 0.003μF as given in IEEE standard [9].

6) Distribution Network

The distribution network downstream of 132kV substations is modelled as parallel pure resistive, inductive, and capacitive elements. The capacitive element represents the total cables' capacitive connected downstream of 132kV substations, and values were obtained from the detailed distribution network model. The parallel resistive and inductive elements represent the aggregated load at the 132kV substation. The values were calculated from the active and reactive power of the aggregated load using Method 2 reported in [5,10-11]. Although the full distribution network model is available, the author chose to employ an equivalent model for the studies reported in this paper to provide the entire network for validation and further research and not be restricted by third-party data confidentiality. As a way of validation for the equivalent model, several EMT simulation studies were carried out using the whole distribution network, and the results were compared to the results from the derived equivalent. The highest difference in the maximum overvoltage values at observed nodes between the two models was around 2.7%.

7) Surge Arrestor

Surge arrestors are represented as nonlinear resistance. Stray capacitance and inductance were not considered.

C. DIgSILENT PowerFactory EMT simulations

The shortest cable section was more than 300m, and the shortest overhead line section was more than 600m; hence, EMT simulations to observe overvoltage were carried out using a 2μs step size.

IV. Energization EMT Studies

Several case studies were performed to examine overvoltage and overvoltage propagation due to the energisation of the three cables, and instantaneous voltage was observed at all nodes within the reduced network. The cases were formulated by considering different planned outage conditions for the cables, synchronised switching (simultaneous three-pole switching) and asynchronized switching, and energisation from each end, i.e., Node A and Node D. In this paper, 5 cases of CCT3 energisation are reported as described in TABLE I. The second column describes the outage (out of service) of relevant circuits at the time of energisation.

TABLE I
DESCRIPTION OF REPORTED ENERGISATION CASES OF CCT3

Case	Network configuration	Energisation
Case 1	Outage of CCT1&CCT2	Synchronised switching from Node A
Case 2	Outage of CCT1	Synchronised switching from Node A
Case 3	CCT1&CCT2 in service	Synchronised switching from Node A
Case 4	Outage of CCT1&CCT2	Asynchronized switching from Node A
Case 5	Outage of CCT1	Synchronised switching from Node D

A. Results

Switching of circuit breakers was executed at 3 different switching angles over a half cycle (every 4ms). TABLE II shows the highest observed V_{ph} and V_L voltages for 400kV nodes within the studied network as per unit calculated using a 420kV base.

TABLE II
INSTANTANEOUS V_L and V_{ph} OBSERVED AT 400kV NODES IN PER UNIT BASED ON 420kV FOR ENERGIZATION

Node		Case 1	Case 2	Case 3	Case 4	Case 5
Node A	V_{ph}	1.2	1.2	1.1	1.2	1.2
	V_L	1.3	1.2	1.1	1.3	1.3
Node B	V_{ph}	1.3	1.2	1.3	1.3	1.5
	V_L	1.4	1.2	1.3	1.3	1.5
Node C	V_{ph}	1.3	1.3	1.2	1.3	1.4
	V_L	1.3	1.4	1.2	1.3	1.4
Node D	V_{ph}	N/A	1.3	1.2	N/A	1.1
	V_L	N/A	1.4	1.3	N/A	1.3
Node F	V_{ph}	2.1	2.4	1.5	1.8	1.5
	V_L	2.2	2.3	1.5	2.0	1.7
Node T	V_{ph}	1.5	1.4	1.2	1.4	1.4
	V_L	1.5	1.5	1.3	1.5	1.5

The first significant observation from the table is that Node F has always experienced the highest overvoltage among all nodes, which has, in some cases, exceeded National Grid TOV limits, i.e., 2 pu. Secondly, the overvoltage values at Node F change significantly with the network configuration and cables' outage. This is clear when comparing results from Case 2 and Case 3. Node T has also experienced high overvoltage compared to other nodes but does not change with configuration nor exceed the limits. When comparing Case 1 and Case 4, synchronised switching gave a higher overvoltage than asynchronized switching. In 40% of simulated cases, Node F experienced overvoltage values that were above TGN 288 limits for V_L voltage, V_{ph} voltage or both. The highest overvoltage occurred when energising CCT3 from Node A when CCT1 is out of service, i.e., Case 2. In this case, energising at any point in time has resulted in the violation of TGN 288 limits; however, no violation of TS 1 limits was observed in any of the cases. The instantaneous V_{ph} for Node A and Node F when simulating Case 2 is shown in Fig. 3, which along with TABLE II demonstrates the transfer and amplification of the switching overvoltage to Node F.

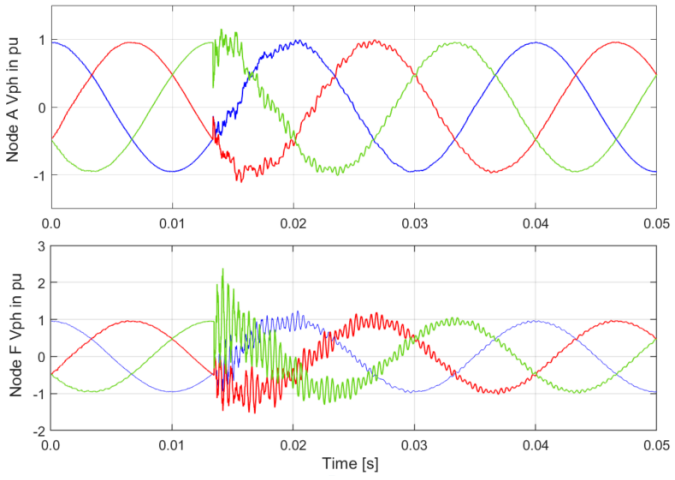

Fig. 3. V_{ph} at Node A and Node F observed in Case 2 simulation

To ensure that the highest overvoltage values were observed

for case 2, i.e., worst case, 80 statistical switching simulations were performed for case 2. Switching time was randomly sampled over a one-cycle period (5ms-25ms), assuming a uniform distribution. Fig. 4 shows the distribution of V_{ph} at Node F for case 2 using 80 switching time samples. The figure shows that the overvoltage values in 78 out of 80 simulations were above the TGN288 limits, i.e., 2 pu, and the remaining 2 cases are at 2 pu. It was also shown that the maximum overvoltage value is 2.4 pu, which was reported in the previous section.

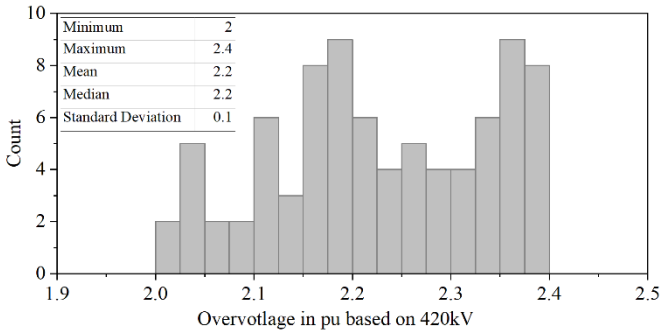

Fig. 4. Distribution of V_{ph} at Node F observed in Case 2 simulations using 80 statistical switching simulations

V. Fault Inception and Clearance Studies

For fault inception and clearance studies, short circuit events were applied at each end of the three circuits and cleared by opening circuit breakers and tripping the circuit. The opening of the circuit breakers was simulated at the zero-crossing point of the current, at a chopping current of 5A, and at a chopping current of 10A. Since CCT2 is a hybrid circuit and faults are more likely to occur on the OHL part; hence more focus is given to this circuit, where 4 cases of fault inception and clearance were simulated as described in TABLE III. In the initial steady state of all 4 cases, CCT1, CCT2, and CCT3 were kept in service.

TABLE III
DESCRIPTION OF REPORTED FAULT CASES OF CCT2

Case	Fault location	Fault Type	Clearance
Case 1	Node A	Single phase to ground	At 10A chopping current
Case 2	Node A	3 phase to ground	At 10A chopping current
Case 3	Node D	Single phase to ground	At 10A chopping current
Case 4	Node D	3 phase to ground	At 10A chopping current

A. Results

Similar to energisation cases, fault inception was simulated at 3 different points in time to capture the worst-case overvoltage values. TABLE IV shows the highest observed V_{ph} and V_L voltages for 400kV nodes within the studied network as per unit calculated using a 420kV base. The values shown in the table are the highest observed overvoltage values during the whole simulation, i.e., fault inception and clearance. However, the fault clearance did not lead to high overvoltage across the entire network, and all values reported in the table are due to fault inception except for Node A and Node D, where the overvoltage occurs at the fault clearance condition. As can be seen, Node F experiences the highest overvoltage values among all nodes. Also, a 3-phase-to-ground fault at Node D causes noticeably high transient overvoltage values at all nodes. For Node F specifically, the overvoltage values (V_{ph}=926 kV and V_L=1485 kV) are close to TS 1 limits, i.e., tested rating of equipment (SIL), and certainly above TGN 288 limits, which is illustrated in Fig. 5. Although these levels of transient overvoltage are compliant with TS 1, they must be seriously taken as the case studies reported in this paper are samples of so many other network configurations and operational scenarios which could lead to higher overvoltage and flashover situations.

TABLE IV
INSTANTANEOUS V_L and V_{ph} OBSERVED AT 400kV NODES IN PER UNIT BASED ON 420kV FOR FAULT CASES

Node		Case 1	Case 2	Case 3	Case 4
Node A	V_{ph}	1.3	1.4	1.2	1.3
	V_L	1.2	1.3	1.1	1.2
Node B	V_{ph}	1.1	1.1	1.3	1.4
	V_L	1.1	1.2	1.3	1.5
Node C	V_{ph}	1.1	1.1	1.4	1.8
	V_L	1.1	1.1	1.4	1.7
Node D	V_{ph}	1.3	1.4	1.2	1.3
	V_L	1.2	1.3	1.1	1.2
Node F	V_{ph}	1.8	1.6	1.9	2.7
	V_L	1.6	1.4	1.7	2.5
Node T	V_{ph}	1.1	1.1	1.7	1.7
	V_L	1.1	1.1	1.7	1.7

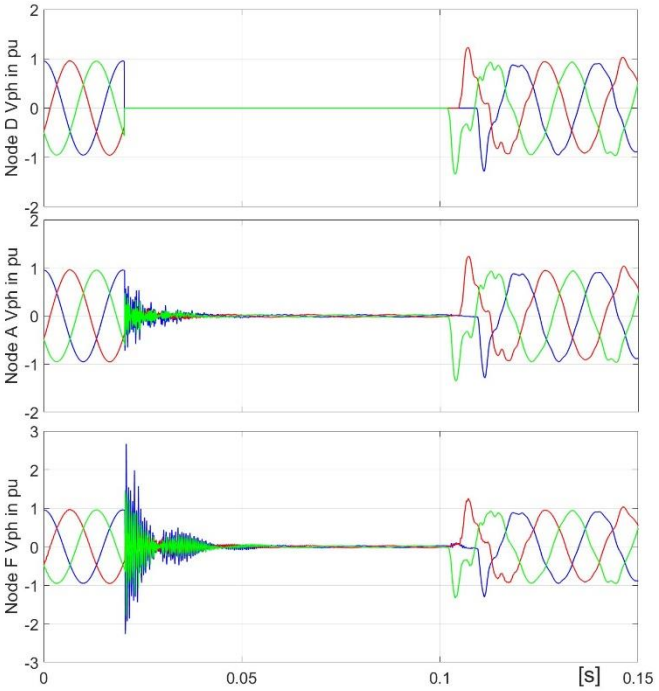

Fig. 5 Vph voltage at Node D, Node A and Node F when a three-phase fault was applied at Node D and cleared at 10A chopping current

With respect to fault clearance, simulation results showed that the overvoltage remains within TGN 288 limits even at Node F for both V_{ph} and V_L voltages, as can be seen in Fig. 5. It is apparent that fault clearance simulated by disconnecting the faulty circuit does not cause any overvoltage values that violate TGN 288 or TS 1 limits.

VI. Frequency Domain Analysis

A. Frequency Scan

To explore the causes of the high overvoltage values at the remote Node F, frequency scans of the self-impedance at Node A, Node D, and Node F, as well as the transfer impedance between the nodes, were obtained using DIgSILENT built-in

function. The scan was carried out for different network configurations and for a frequency range of 50 Hz to 3.5 kHz. Since the observed issue is mainly about transfer and propagation of overvoltage, transfer coefficients from Node A and Node D to Node F were acquired by dividing the transfer impedance between nodes by the self-impedance of Node A or Node D, e.g., for the transfer coefficient between Node A and Node F, dividing the transfer impedance between Node A and Node F by the self-impedance of Node A. TABLE V explains the network cases for frequency scan assessment where Case 1 to Case 3 are the same network configurations for Case 1 to Case 3 given in TABLE III and Case 4 is the network scenario used to perform fault inception. Fig. 6 and Fig. 7 show transfer coefficients from Node A to Node F and from Node D to Node F, respectively.

TABLE V
FREQUENCY SCAN CASES TO OBTAIN TRANSFER COEFFICIENTS

Case	Network configuration
Case 1	CCT1, CCT2, CCT3 are out of service
Case 2	CCT1 and CCT3 are out of service (CCT2 is in service)
Case 3	CCT3 is out of service (CCT1 and CCT2 are in service)
Case 4	CCT1, CCT2, CCT3 are in service

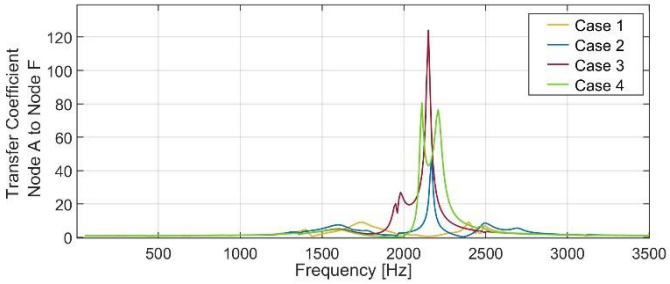

Fig. 6. Transfer coefficient from Node A to Node F at different frequencies

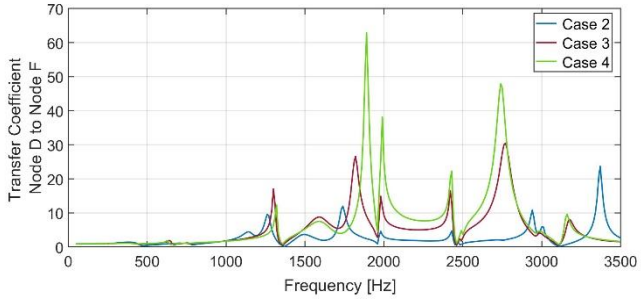

Fig. 7. Transfer coefficient from Node D to Node F at different frequencies

Fig. 6 confirms a resonance condition at around 1700 to 2500 Hz between Node A and Node F. For transfer coefficients from Node D to Node F, there are several resonance peaks across a wide frequency range (1200 Hz-3500 Hz); however, the magnitudes are lower than transfer coefficients from Node A to Node F, as seen in Fig. 7. This means that a switching event causes transient voltages with a wide frequency content which in turn excite these resonances, some of which would be greatly amplified at Node F.

B. Fast Fourier Transformation

To get more insight into the resonance conditions shown in the previous section, Fast Fourier Transform (FFT) analysis was carried out to check for the presence of dominant frequency components that are in the resonance range identified by the transfer coefficients. FFT was applied on the waveforms shown in Fig. 3 over a half-cycle window (10ms) at the beginning of the time of energisation. Fig. 8 shows the obtained FFT magnitude of Phase C's V_{ph} in pu based on 400kV (the phase with the highest overvoltage shown in green in Fig. 3) for both Node A and Node F. The FFT figure does not include the fundamental frequency (50Hz). The major observation is the noticeable frequency components in the frequency range 1800-2500 Hz which to some degree matches the resonance profile identified by the transfer coefficient in Fig. 6. The gain between Node A and Node F at the individual frequency can be calculated by dividing the frequency component magnitude at Node F by the magnitude at Node A. Fig. 9 shows a comparison between the gain calculated from FFT and the transfer coefficient of Case 2, which visibly demonstrates the great match of the resonance profile.

Note that the FFT with a defined window length is used here for the indication and identification of dominant components within the signal; therefore, the calculated magnitudes should not be used for comparison with the limits or selection of equipment rating. Furthermore, since the same FFT window length is applied to both voltage signals at Node A and Node F, the results are deemed to be valid for comparison purposes only. Further explanation on this point will be given in Section D. Discussion.

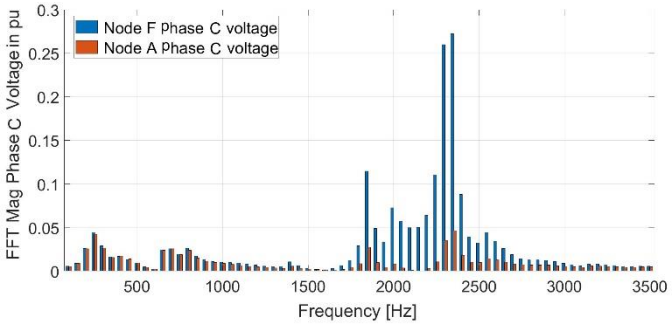

Fig. 8. Frequency analysis using FFT for the waveform shown in Fig. 3

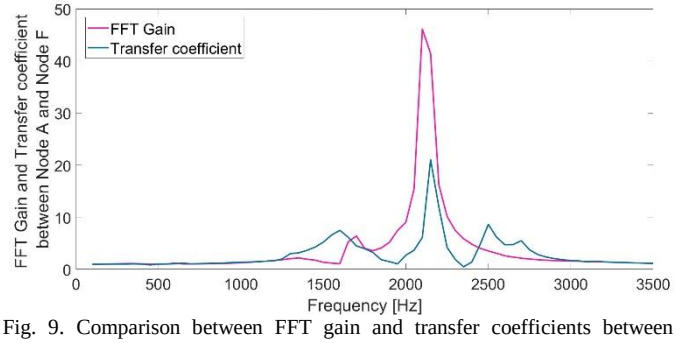

Fig. 9. Comparison between FFT gain and transfer coefficients between Node A and Node F for Case 2

The same FFT analysis was applied to the waveform obtained from simulating Case 5 described in TABLE II where energisation of CCT3 was performed from Node D. Fig. 10 shows the obtained FFT magnitude of Phase A V_{ph} for Node D (the energisation side) and Node F. Fundamental frequency component is not included in the figure. The highest amplification values of frequency components are between 1700Hz-1850Hz, which matches one of the resonance peaks shown in Fig. 7.

As a way of comparison, the frequency components of the waveform at Node D (given in Fig. 10) were used to calculate the frequency components at Node F using the transfer

coefficient obtained from the frequency scan. This was achieved by multiplying individual frequency components by individual transfer coefficients. Fig. 11 shows the two sets of frequency components at Node F; 1) calculated using transfer coefficient and 2) obtained from simulation results using FFT. As can be seen, the two sets match very well, which confirms that the resonance between the two nodes leads to amplification and high overvoltage at Node F. Note that there are frequency components with high discrepancy. The differences between the calculated and simulated components are attributed to the selection of FFT window, spectral leakage and averaging nature of the FFT process, which averages the signal within the window, which in turn leads to inaccuracy of the magnitude of the FFT output for a decaying-with-time signal.

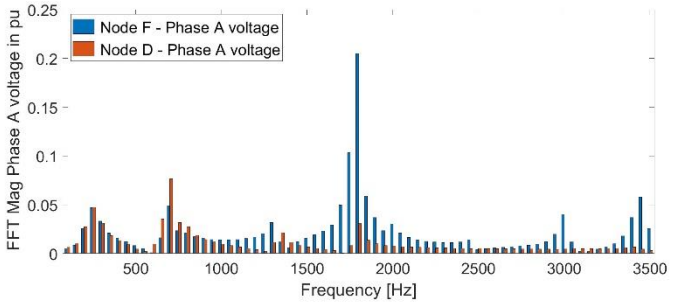

Fig. 10. Frequency analysis using FFT for Phase A voltage waveform obtained from simulating Case 5 in TABLE II.

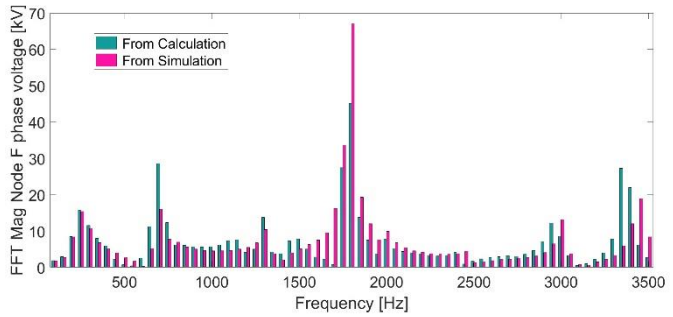

Fig. 11. Frequency components of Node F Phase A voltage in kV calculated using transfer coefficient and obtained directly from waveform using FFT

C. Bus Impedance Matrix

To investigate the impact of network conditions on the resonance and the frequency components, and hence the occurrence of amplification, the bus impedance matrix at 2150 Hz (the frequency with the highest transfer coefficient and FFT gain shown in Fig. 9) for Case 2 and Case 3 described in TABLE I are shown below. Although in the two cases, the same circuit was energised from the same end at Node A, the results were so different as Case 2 leads to overvoltage non-compliance, and in Case 3, overvoltage values were below the limits.

1) Bus Impedance Matrix - Case 2 at 2150 Hz

$$\begin{matrix} Node\ D \\ Node\ A \\ Node\ F \end{matrix}\begin{bmatrix} 66.3\angle -87 & 1.9\angle -153 & 166\angle 88 \\ 1.9\angle -153 & 5.3\angle -72 & 111.3\angle -100 \\ 166\angle 88 & 111.3\angle -100 & 1950\angle 75 \end{bmatrix}\Omega$$

2) Bus Impedance Matrix - Case 3 at 2150 Hz

$$\begin{matrix} Node\ D \\ Node\ A \\ Node\ F \end{matrix}\begin{bmatrix} 41.6\angle -83 & 9.0\angle -93 & 215.3\angle 96 \\ 9.0\angle -93 & 0.5\angle 0 & 63.8\angle -88 \\ 215.3\angle 96 & 63.8\angle -88 & 1276\angle -84 \end{bmatrix}\Omega$$

From the above bus impedance matrices, the self impedances at Node A for Case 2 and Case 3 are 5.3∠-72 and 0.5∠0 Ω. The transfer impedances between Node A and Node F are 111.3∠-100 and 63.8∠-88 Ω. These lead to transfer coefficients of 21 and 127.6 for Cases 2 and 3, respectively. The overvoltage produced at Node A is lower in Case 3 than in Case 2. This is evident in Fig. 12 as compared to Fig. 3, where the voltages are less noisy due to a reduction in the dominant frequency component magnitude. The transfer impedance between the two nodes is also smaller in Case 3, resulting in lower transferred voltage to Node F. Low self and transfer impedances result in lower voltages at that frequency component at Node A and lower propagation of that frequency component to Node F, despite higher transfer coefficient for Case 3. Therefore, it can be concluded that the higher transfer coefficients may not necessarily lead to high overvoltage values at remote nodes.

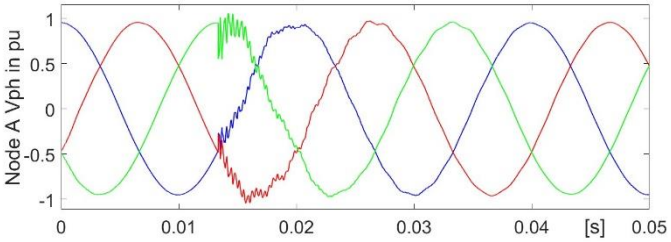

Fig. 12. V_{ph} at Node A observed in Case 3 simulation

To investigate the existence of similar high transfer coefficient values between Node A and other nodes, frequency scans were performed to obtain the transfer impedance between the nodes. Expectedly, the results of these scans did not show a similar pattern to the one observed between Node A, Node D, and Node F. For example, Fig. 13 compares the transfer coefficient from Node A to Node F and from Node A to Node C for Case 2 (NB: Node C experienced the lowest overvoltage under Case 2). As seen in the figure, for the transfer coefficient between Node A and Node C there are no peaks in the frequency range where FFT analysis showed high values of frequency components in Node A waveform (1900 - 2500 Hz). Also, the high transfer coefficient value at 3100 Hz shown in Fig. 13 did not cause overvoltage amplification as the frequency component value was insignificant, as shown in Fig. 8.

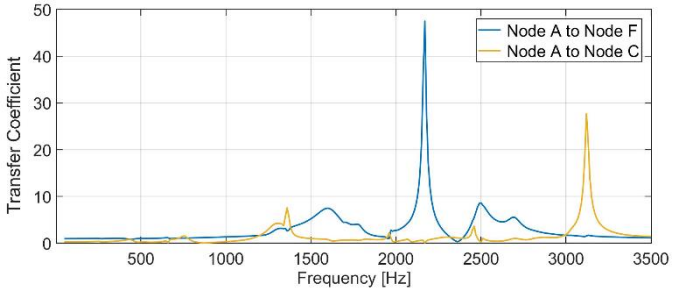

Fig. 13. Transfer coefficient from Node A to Node F and from Node A to Node C for Case 2 at different frequencies

D. Discussion

The results in sections III and VI demonstrate the propagation and amplification of overvoltage in the 400kV network, especially at Node F. The observed overvoltage at Node F matched a historical incident where the LV side of one

of the transformers at Node F flashed over when one of the cables was switched in. Frequency analysis results, including frequency scan and FFT, indicate the presence of resonance at a specific frequency range that matches the range of the largest frequency components of the transient overvoltage waveform. Although the values of the gain obtained from FFT and transfer coefficient are not identical, the frequency profiles of both are comparable for all case studies. The difference in the values is most likely due to the waveform time window that is used to perform FFT and possible spectral leakage due to the aperiodic nature of the waveform, and the difference in frequency dependency application of damping in time and frequency domain for transformers', lines', and cables' models. In addition, the transfer coefficient was obtained using a balance frequency scan, i.e., including only positive phase sequence impedance, while the FFT was obtained from the EMT simulation which includes the unbalance nature of the network, e.g., untransposed lines and thus both positive and zero phase sequence impedances. Results also indicate that energising the new cables causes switching transient overvoltage propagation but does not initiate TOV at the event node or at remote nodes.

VII. Mitigation Options

There are mitigation options to reduce transient overvoltage, for example, installing surge arrestors or using a pre-insertion resistor. However, the mitigation option for switching overvoltage used by National Grid is the installation of surge arresters at the non-compliant substations. The surge arrester option is also suitable for overvoltages caused by fault inception.

There are existing surge arresters at Node A (two at the shunt reactors and one at the low voltage side of one of the transformers) and at Node F (at the high and low voltage sides of one of the transformers). In addition, surge arresters will be installed at Node A as part of the replacement project. The V-I characteristic of these surge arresters was adopted from the standard type-registered design by National Grid with a minimum rated voltage of 360 kV. However, when carrying out the studies, these surge arresters did not mitigate the non-compliant cases, as shown previously. Therefore, there was a need to explore different surge arrester designs, i.e., V-I characteristics, to determine the most suitable one. Two models from ABB, a) EXLIM Q-D rated at 360 kV and b) EXLIM T rated at 330 kV were employed [13], with Q-D model matching the recommended specifications by National Grid. Moreover, an additional surge arrester was modelled at the high voltage side of the second transformer connected at Node F.

Energisation and fault inception studies were repeated using the two designs of surge arresters separately. The results for energisation Case 2 and fault inception Case 4 (the worst overvoltage at Node F) are given in TABLE VI. For V_{ph} voltage, both surge arrester designs bring V_{ph} voltage at or under TGN 288 limits. For V_L voltage, only 330kV surge arrester mitigates non-compliance overvoltage and brings it under the limits. The energy absorbed by both surge arresters in all cases did not exceed the thermal energy rating (W_{th}) shown in TABLE VII. In fact, the energy absorbed did not exceed 1% of the rated thermal energy of both surge arresters.

TABLE VI
VOLTAGE OBSERVED AT NODE F WITH DIFFERENT SURGE ARRESTER MODELS – ENERGIZATION & FAULT INCEPTION

Case		Base case	Q-D360	T330
Energization - Case 2	V_{ph}	2.4	2.0	1.8
	V_L	2.3	2.1	1.9
Fault Inception - Case 4	V_{ph}	2.7	2.0	1.8
	V_L	2.5	2.2	2.0

TABLE VII
ENERGY ABSORBED BY THE TWO TYPES OF SURGE ARRESTER – ENERGISATION & FAULT INCEPTION

Surge Arrester	Rated Energy [kJ]	Absorbed Energy [kJ]	
		Energisation – Case 2	Fault Inception – Case 4
Q-D360	2880	17.9	27.6
T330	4950	28.9	36.0

It must be noted that National Grid's technical specification for surge arrester states that the minimum surge arrester-rated voltage for 400 kV should be 360 kV, and hence the design rated 330kV does not meet the requirement. However, the results of these studies clearly demonstrate that models that meet the recommended specifications by National Grid do not mitigate the amplified overvoltage at Node F. The available options, in this case, would be to derogate from the technical specification.

VIII. Conclusions

Electromagnetic Transient (EMT) studies were carried out to investigate overvoltage propagation in a 400kV network that was known for switching transient overvoltage issues. The studies simulated energisation and fault inception and clearance for three new cables to examine compliance against National Grid's specifications and limits.

The most significant finding of the investigation is that events such as energisation or fault inception involving new cables, lead to overvoltage values at remote nodes that are close to switching withstand voltage for instantaneous voltage. The frequency scan studies show a resonance condition between the point of event and the remote nodes for a specific frequency range which cause the amplification of the overvoltage values. Results also indicate that energising or fault inception on the new cables cause switching transient overvoltage amplification but do not initiate TOV at the event node or at other nodes within the network. Surge arresters were proven to mitigate the overvoltage effectively, and brought value within limits.

The paper provides an example of overvoltage propagation on a realistic 400kV transmission network.

IX. Appendix A

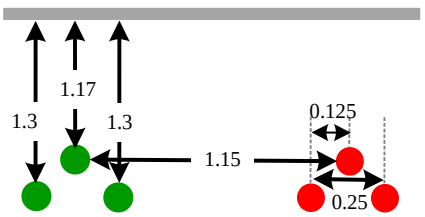

Fig.A-1. Cable layout dimensions in meters

TABLE A-I
CABLE CORE DATA

	Conductor	Sheath	Insulation	Over-sheath
Material	Copper	Aluminum	XLPE	PE
Thickness [mm]	32.65	1.4	26.4	5

TABLE A-II
CABLES SECTIONS AND TRENCH COUPLING

Sections	CCT1 [km]	CCT2 [km]	CCT3 [km]	Same Trench
Section 1	0.84	0.95	0.95	Circuit-2 & 3
Section 2	0.95	0.95	0.95	Circuit-1 & 2
Section 3	0.985	0.985	0.83	Circuit-1 & 2
Section 4	1	1	0.635	Circuit-1 & 2
Section 5	0.68	0.68	0.53	Circuit-1 & 2
Section 6	0.96	0.96	0.53	Circuit-1 & 2
Section 7	0.96	0.96	0.95	Circuit-1 & 2
Section 8	1.08	1.082	0.95	Circuit-1 & 2
Section 9	0.95	N/A	0.95	circuit-1 & 3
Section 10	0.95	N/A	0.95	circuit-1 & 3
Section 11	0.95	N/A	0.95	circuit-1 & 3
Section 12	0.95	N/A	0.95	circuit-1 & 3
Section 13	0.52	N/A	0.48	N/A

Cross-bonding of the sheath is applied between sections for the three circuits. For CCT2, only earthing at both ends is applied, i.e., no earthing at any section is used. For CCT1 and CCT3, earthing via a sheath voltage limiter (SLV) is employed after every 3 sections (sections 3, 6, 9, and 12).

TABLE A-III
CABLE EQUIVALENT (RXB) DATA

Circuit	R^+ Ω/km	X^+ Ω/km	B^+ μF/km	R^0 Ω/km	X^0 Ω/km	B^0 μF/km
Node A-Node T	0.01	0.17	70.78	0.15	1.31	70.78
Node B-Tee	0.02	0.19	59.69	0.16	1.96	103.3

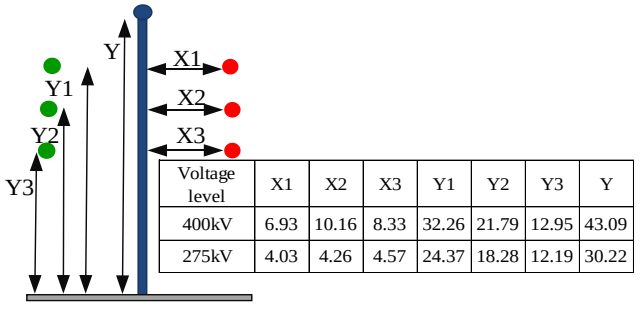

Voltage level	X1	X2	X3	Y1	Y2	Y3	Y
400kV	6.93	10.16	8.33	32.26	21.79	12.95	43.09
275kV	4.03	4.26	4.57	24.37	18.28	12.19	30.22

Fig.A-2. Overhead lines tower structure and dimensions

TABLE A-IV
OVERHEAD LINES CONDUCTOR AND EARTH WIRE PARAMETERS

	Conductor				Earth Wire	
Voltage level kV	Outer diameter	R-DC Ω	No Bundle	Bundle distance cm	Outer diameter	R-DC Ω
400	28.62	0.067	4	30	28.62	0.064
275	19.53	0.158	2	30	19.53	0.158

TABLE A-V
DISTRIBUTION NETWORK EQUIVALENT PARAMETERS

	R [kOhm]	L [H]	C [μF]
Node A	1.96	17.74	3.07
Node F	1.00	6.70	5.00
Node T	9.57	2.88	1.23

TABLE A-VI
THEVENIN EQUIVALENTS FOR REDUCED NETWORK

Node	Voltage V_L kV	Voltage deg	R1 Ohm	X1 Ohm	R0 Ohm	X0 Ohm
Node B	404	-29.5	33.9	167.6	0.2	31.4
Node C	404	-28.9	2.5	20.7	2.2	22.2
Node T	404	-28.9	4.2	68.1	7.3	62.8

TABLE A-VII
NETWORK TRANSFORMERS DATA

Tx	MVA	HV-MV		MV-LV		LV-HV	
		X [%]	Pc[W]	X [%]	Pc[W]	X [%]	Pc[W]
Node T	1000	16.8	1320	6	358.2	7.3	437
	750	12.5	1184	6.1	50	7.9	80
Node T2	120	14.7	410	N/A	N/A	N/A	N/A
	120	14.7	410	N/A	N/A	N/A	N/A
Node F	240	20.1	708	7.4	145.2	12.8	144
	240	19.9	869	5.6	100	10.7	120
Node A	240	19.4	934	7.4	141.3	13.3	145
	240	20.2	847	6.8	141.3	12.7	145

TABLE A-VIII
TRANSFORMERS SATURATION CURVE

	Knee Flux pu	Linear Reactance pu	Saturated Reactance pu	Saturation Exponent
Node T	1.1	2305.635	0.45	21
	1.1	2305.635	0.45	21
Node T2	1.1	83.649	0.00	3
	1.1	83.649	0.00	3
Node F	1.1	731.835	0.09	21
	1.1	2092.061	0.08	21
Node A	1.1	3213.208	0.08	21
	1.1	1396.018	0.09	21

X. REFERENCES

[1] R. Gerald Colclaser, C. Wagner and D. Buttner, "Transient Overvoltages Caused by the Initiation and Clearance of Faults on a 1100-kV System," *IEEE Transactions on Power Apparatus and Systems*, Vols. PAS-89, no. no. 8, pp. 1744-1751, 1970.

[2] S. Aparcio, A. Pizzini, H. Saad and S. Deschanvres, "Switching overvoltages studies for Live Working on the Uruguayan 500 kV transmission network," in *International Conference on Power System Transient*, Perpignan, France, 2019.

[3] National Grid, *Ratings and General Requirments for Plants, Equipment and Apparatus Directly Connected to National Grid System, TS 1 (RES)*, issue1, 2018.

[4] National Grid TGN(E) 288, "nationalgrid.com," May 2016. [Online]. Available: https://www.nationalgrid.com/sites/default/files/documents/TGN%28E%29_288_0.pdf. [Accessed October 2022].

[5] IEC TR 60071-4, "Computational guide to insulation co-ordination and modelling of electrical networks," *IEC Standard*, 2004.

[6] I. Kocar and J. Mahseredjian, "Accurate Frequency Dependent Cable Model for Electromagnetic Transients," *IEEE Transactions on Power Delivery*, vol. 31, no. 3, pp. 1281-1288, 2015.

[7] Z. Gajic, B. Hillstrom and F. Mekic, "HV Shunt Reactor Secrets for Protection Engineers," in *30th Western Protective Relaying Conference*, Spokane, 2003.

[8] A. Khursheed, F. Ghassemi, P. Haigh, F. Moore, D. Aik, J. Peng and K. Smith, "A Transmission Utility Approach to Electromagnetic Transient Analysis," in *International Conference on Power Systems Transient (IPST2015)*, Cavtat, Croatia, 2015.

[9] IEEEStd C37.015, "IEEE Guide for the Application of Shunt Reactor Switching," 2017.

[10] JWG C4/B4.38 Cigre TB 766, "Network modelling for harmonic studies", Cigre TB, 2019

[11] R. Burch et al., "Impact of aggregate linear load modeling on harmonic analysis: a comparison of common practice and analytical models," in IEEE Transactions on Power Delivery, vol. 18, no. 2, pp. 625-630, April 2003, doi: 10.1109/TPWRD.2003.810492.

[12] ABB, "High voltage surge arrester - Buyer's guide," 2019.